International Journal of Mechanical and Production Engineering Research and Development (IJMPERD)
ISSN(P): 2249-6890; ISSN(E): 2249-8001
Vol. 9, Issue 3, Jun 2019, 645-654
© TJPRC Pvt. Ltd.

NUMERICAL INVESTIGATION ON THE DRAG CHARACTERISTICS OF AUV HULLS

HIMANSHU UPPAL[1], MANOJ T ISAAC[2] & SHAMEEM. B. M[1]

[1]*Department of Naval Architecture and Offshore Engineering, Academy of Maritime Education and Training, Chennai, Tamil Nadu, India*

[2]*Department of Ship Technology, Cochin University of Science and Technology (CUSAT) Kochi, Kerala, India*

ABSTRACT

Autonomous Underwater Vehicles (AUVs) are self-propelled robotic platforms that carry a suite of instruments and sensors which enable the vehicle to navigate the depths of the ocean using its onboard power. Due to the limited power onboard the vehicle, efficient streamlining is an important design consideration for maximum endurance of a cruising type AUV. Torpedo-shaped hull forms are very common among cruising type AUVs, which consist of a nose section, a cylindrical mid-body section, and a tail section. This paper discusses different torpedo-shaped bare-hulls formed by changing the nose and tail sections to identify which combination of nose and tail renders the most hydrodynamically efficient hull form. A torpedo-shaped AUV bare-hull for which experimental results were available is selected as the base model and CFD analysis is performed and validated. With the validated CFD model, the different shaped hull configuration is changed by modifying its nose and tail profiles. A total of seven configurations were analyzed for three different speeds. The least drag shaped configuration is identified and recommended for further inclusion of control surfaces.

KEYWORDS: AUV, CFD, Drag & Torpedo-Shape

Received: Mar 19, 2019; **Accepted**: Apr 09, 2019; **Published**: May 06, 2019; **Paper Id**.: IJMPERDJUN201971

Original Article

Nomenclature

F_D	Drag force (N)
X	Length (m)
R	Maximum radius of nose profile (m)
N	Nose index
Θ	Semi-tail angle
U	Speed (m/s)
C	Tail length (m)
T	Time (s)
Ω	Total control volume bounded
A	Total length of nose (m)
V	Volume of displacement of the hull (m^3)
C_{dv}	Volumetric Drag Coefficient

1. INTRODUCTION

An Autonomous Underwater Vehicle (AUV) is a self-propelled robotic vehicle controlled and piloted by an onboard computer, which is capable of maneuvering in 3D space without the supervision of an operator. Under

most environmental conditions the vehicle can follow precise pre-programmed trajectories. Sensors onboard the AUV sample the water column, providing the ability to make both spatial and time series measurements. Data collected by an AUV is automatically geospatially and temporally referenced and normally of superior quality. Multiple vehicle surveys can increase productivity and insure adequate temporal and spatial sampling thereby provide a means of investigating the coherence of the ocean in time and space [1]. AUVs find application in various fields such as research, oil exploration, defense purpose, etc. Underwater vehicles fall into two basic categories: (a) Manned and (b) Unmanned. The manned versions include submarines and passenger carrying submersibles. The costs and risks associated with the manned underwater vehicles are more that in the recent past decades there has been an obvious trend toward unmanned vehicles. Unmanned underwater vehicles include towed vehicles, ROVs and AUVs. A towed vehicle normally does not have any propulsion system and is generally connected to vessel by a cable. An ROV is a tethered vehicle but has thrusters for maneuvering in 3D space and generally controlled by an operator from a surface ship. In addition, they are powered through tethers and transfer of data is established from the vessel operator to receive commands during its operations. As far as AUVs are concerned, they are not connected by tethers or cables for its operation during a mission. The fact that AUVs are untethered brings in the necessity for onboard power on an AUV. Hence, the endurance of an AUV is limited by the battery power they carry onboard. An autonomous underwater vehicle is typically designed to operate at a nominal speed range of 0.4 to 2 m/s [2]. Since, the availability of battery power on board is limited, to minimize the powering needs, a streamlined hull-form is generally preferred for a cruising type AUV. This reduces the resistance experienced by the hull in the fluid medium. There are different hull forms but the most common hull-forms preferred for cruising type AUVs are: i) Torpedo shaped profile ii) Low drag profile, Figures 1 and 2

A low-drag profile has the advantage of a more streamlined flow around the body and hence the drag is less. However, constraints like fixed size (lack of modular flexibility) and costlier fabrication constitute the difficulties [12].

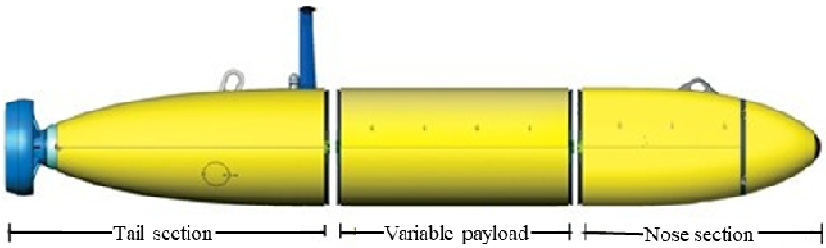

Figure 1: Torpedo Shaped Profile (Nose, Cylindrical Mid-Body, Tail), [7]

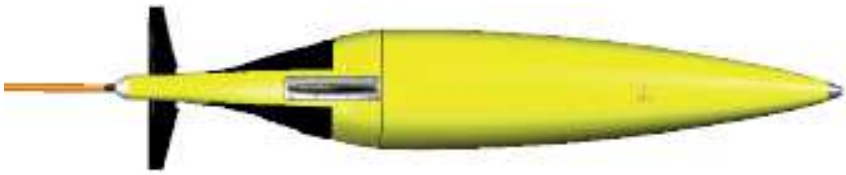

Figure 2: Low Drag Streamlined Profile (Radius Varies along the Length), Sea-glider [11]

A torpedo-shaped AUV as shown in Figure 1 on the other hand, is modular in design consisting of a forward nose section, a mid-body and an aft tail section. The easy to fabricate cylindrical mid-section and the feasibility of modular interchange outweigh the demerits such as increased drag and structural weight. As hull geometry largely influences the ability of an AUV to efficiently maneuver in the water, the focus of this study is to compare the effect of hull geometry (profile shape) on hydrodynamic efficiency. In this paper, a torpedo-shaped hull is selected and numerical analysis has

been carried out using CFD techniques by modifying the bare hull with a different nose and tail configurations to obtain the hydro dynamically efficient (least drag) profile.

2. METHODOLOGY

The bare hull selected is the standard profile proposed by D. F. Myring with a cylindrical midbody [9]. The bare-hull geometry presented in [6]is taken as the base model, see Figure 3. The equations defining the nose and tail profiles are given below,

$$r(x) = \frac{d}{2}\left[1 - \left(\frac{x-a}{a}\right)^2\right]^{\frac{1}{n}}, (Nose) \quad (1)$$

$$r(x) = \frac{d}{2} - \frac{3d}{2c^2} - \frac{tan\theta}{c}\left(x - l_f\right)^2 + \left[\frac{d}{c^2} - \frac{tan\theta}{c^2}\right]\left(x - l_f\right)^3, (Tail) \quad (2)$$

Where, r = maximum radius of nose profile, a = total length of nose, x= length, n= nose index, α= semi-tail angle, c= tail length *etc.* Variables such as nose index (n), semi-tale angle (θ^0), were identified responsible for the fullness of both nose and tail sections respectively. This model had a semi-elliptical nose profile which confirmed to a shape described by Eq.(1) when the *Myring* parameter n takes a value equal to 2 and the tail is termed as Huang tail [4]. The methodology adopted is to obtain the least drag profile through numerical investigation using CFD. The experimental results available [9] is taken as the reference data.

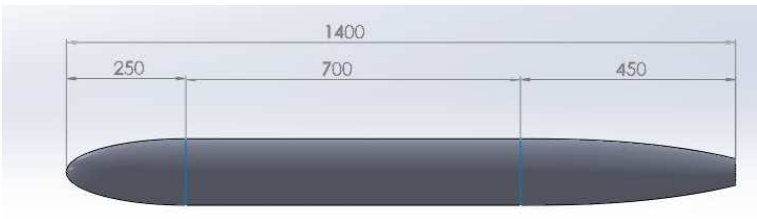

Figure 3: Bare-Hull Geometry (all Dimensions in mm)
Nose Shape Myring, (n=2) with Huang Tail

In the present study, a total of seven different profiles consisting of four different noses and three tails has been configured and analyzed. These different configurations were obtained by changing the parameters n and θ0 in the Myring equation. The configured profiles of nose and tail shapes are shown in Figures 4 and 5 respectively.

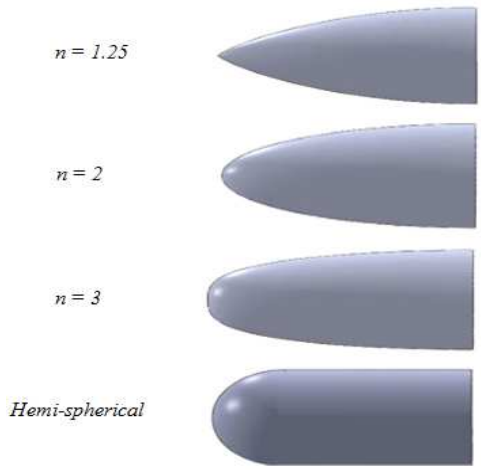

Figure 4: Configured Nose Profiles using Eq (1) and Hemispherical Shape

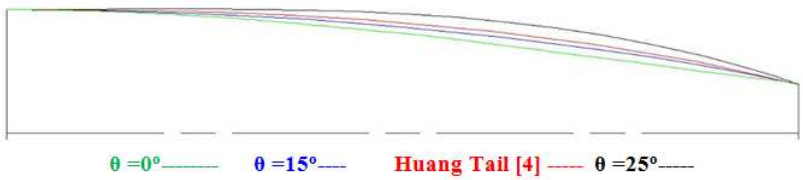

Figure 5: Configured Tail Profiles using Eq. (2)

The analysis has been carried out in three phases. In the first phase, the selected combination and the available experimental results from the literature are validated with CFD. In the second phase, with the validated CFD solver parameters, the nose shape of the same model is being replaced by a different combinations. The AUV hull models of different nose profiles with Huang tail [4] is shown in Figure 6. The low drag nose profile is found from these combinations, i. e., n = 3, and then the tail of the AUV models are replaced by combination of tail profiles as shown in Figure 7. Finally, a least drag hull profile is obtained with a combination of least drag nose and tail profile amongst all models. Total seven profiles are tested in both the stages at different speeds (0.6, 1.0 and 1.4 m/s) and drag coefficients of all the models are compared and tabulated.

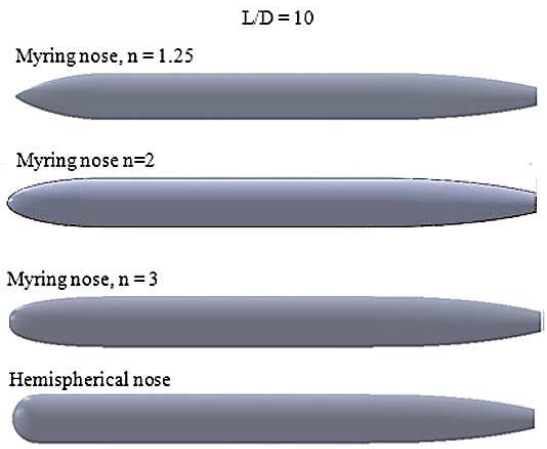

Figure 6: AUV Models with Modified Nose Profiles

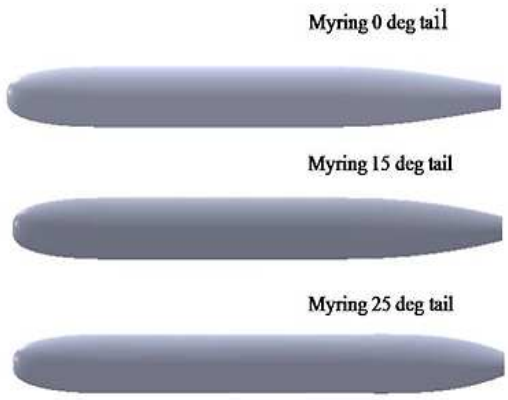

Figure 7: AUV Models with Modified Tail Profiles

3. NUMERICAL MODELING

To investigate the single-phase flow of fluid around the bare hull geometry, RANSE solver has been used for the numerical investigation using the Siemens STARCCM+ module, considering the viscous effects. The equation for RANSE is given below:

$$\frac{dt}{d}\int_{\psi} \rho\varphi dV + \int_{\Gamma} \rho\varphi(v - v_b).ndS = \int_{\Psi} \Gamma\nabla\varphi.\mathrm{ndS} + \int_{\Omega} q_{\theta,v}\,\mathrm{dV} \quad (3)$$

The parameters Ω is total control volume bounded by control surface is given byψ. ‘t’ is time, ρ is the density of the fluid medium, v is velocity vector of fluid.

The computational domain around the bare hull geometry of AUV is taken as shown in Figure 8 where the velocity inlet is at 10D from the nose end in bow, pressure outlet is at 39D from tail end of the bare hull, wall boundaries are at 5D from both in top and bottom and along port and starboard sides. D is the maximum diameter of the bare hull i. e. 0.14m.

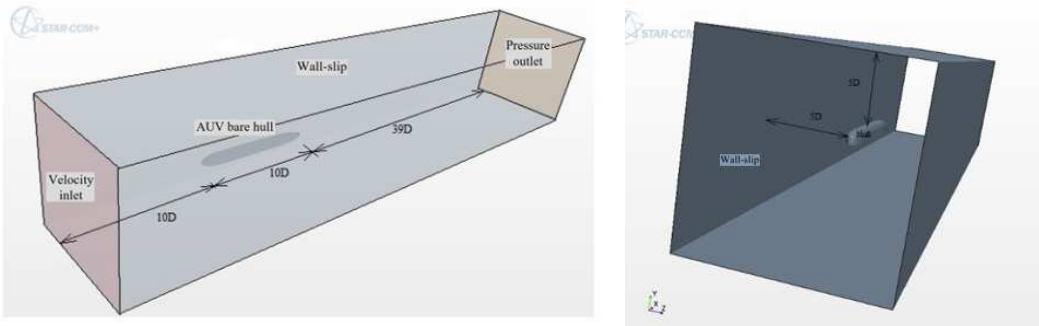

Figure 8: Computational Domain

The domain is divided into three regions for 3D grid generation, the region differs in term of the size of the cells and the associated growth ratio of cell dimensions perpendicular to the surface of the AUV hull. The mesh generated around the hull is shown in the Figures 9 and 10. The boundary conditions used for the computational domain are shown in Table 1.

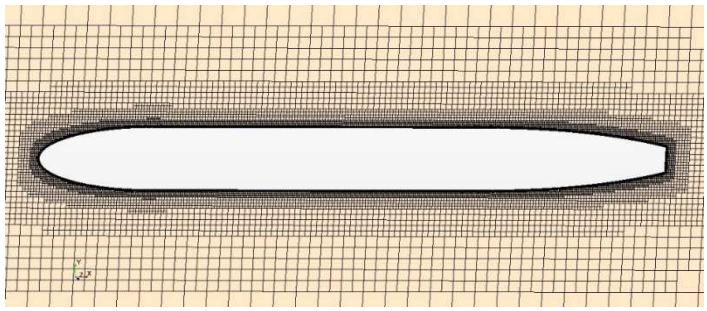

Figure 9: Volume Mesh Generation around the Hull

Figure 10: Volume Mesh Generation on AUV Bare Hull

Table 1: Boundary Conditions for the Computational Domain

Parts	Boundary Condition
AUV bare hull	Wall no-slip
Inlet boundary	Velocity inlet
Outlet boundary	Pressure outlet
Exterior boundary	Wall-slip

4. RESULTS AND DISCUSSIONS

The model [9] is first put into numerical investigation using CFD. The results at three speeds (0.6, 1, 1.4 m/s) are computed and compared with the experimental work for validation. The drag force is obtained from the CFD solver and the results are plotted for the coefficient of drag. The following empirical formulae are used for obtaining the drag

coefficient,

$$C_{dv} = \frac{F_D}{0.5\,\rho\,U\,V^{2/3}} \tag{4}$$

Where C_{dv} is the volumetric coefficient of drag, F_D is the drag force, V is volume (m^3) of displacement of the hull and U is the speed (m/s) and ρ is the density (kg/m^3) of the fluid medium. Next, the hulls are modified with the nose and tail profiles keeping the L/D ratio as 10 for the uniformity and comparison. Due to the changes in the nose and tail profiles, there is minimal variation in overall volume among the AUV models. The CFD results obtained has only a maximum percentage error deviation of 1.45%. Henceforth the domain size and boundaries applied here is considered as the reference for further investigations with different configurations of AUV hulls. The validation of the CFD results and the experimental work from the literature are shown in Figure 11. Table 2 shows the percentage error deviation of the CFD results with the published literature.

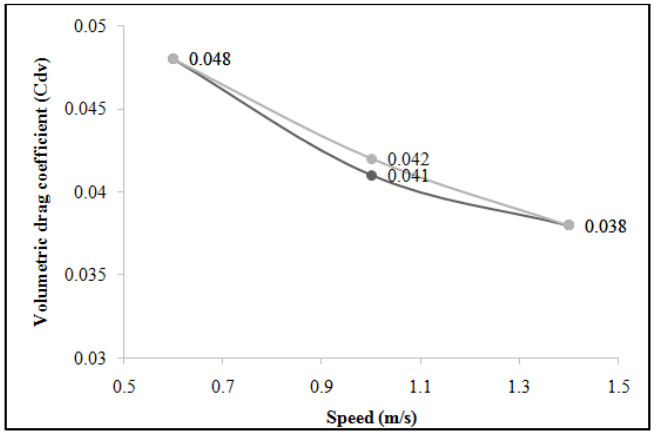

Figure 11: Comparison of CFD Results with the Available Experimental Results

Table 2: Error Comparison of Experiment with CFD Results

Velocity U (m/s)	Experimental Results (Literature)	CFD Results	Deviation %
	C_{dv}	C_{dv}	
0.6	0.0489	0.0481	1.45
1	0.0419	0.0421	0.58
1.4	0.0389	0.0387	0.43

4.1 Comparison Results for Different Nose Profiles

With the validated computational domain, the drag estimation is carried out for different nose profiles with Huang tail combination for the selected speeds. The comparison of these results on the drag coefficient with the modification in the nose is shown in Figure 12 and tabulated in Table 3.

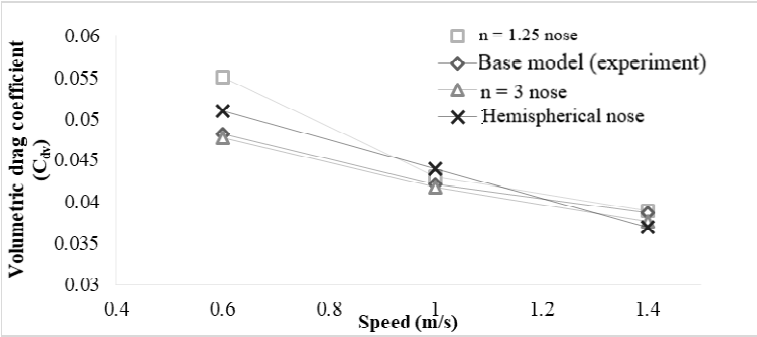

Figure 12: Comparison of the Drag Coefficient for Different Nose Geometry

Table 3: Drag Coefficient Values for Different Nose Profiles

	Drag Coefficient Values for Different Nose Profiles (C_{dv})			
	Base Model (n=2) and Huang Tail	n =1.25	n = 3.0	Hemi-Spherical
0.60	0.0482	0.0550	0.0477	0.0510
1.00	0.0421	0.0430	0.0417	0.0440
1.40	0.0387	0.0390	0.0377	0.0370

It can be seen that for the nose with n=1.25 and Hemispherical shapes, the coefficient of drag is maximum at lower speeds and reduces when the speed increases. In the case of the hemispherical nose, the separation occurred in the forward part due to a sudden change in the geometric profile. But when the speed increases, it is observed that the drag reduced only at the maximum considered speed. From this analysis, it can be stated that the Myring nose, n=3 profile produces less drag constantly moving from lower to higher speeds. An error comparison has been made and tabulated in Table 4 with the base model and the selected nose profile n = 3 for further studies by incorporating the tail sections. The deviation(%) shows that the obtained drag coefficient results from the CFD results for the model with nose profile n=3 is better than all the other profiles.

Table 4: Error Comparison of C_{dv} of Base Profile (Literature) and n=3

Speed (m/s)	Volumetric Drag Coefficient Values (n)		Deviation %
	C_{dv} for n=2	C_{dv} for n=3	
0.60	0.0482	0.0477	1.05
1.00	0.0421	0.0417	0.96
1.40	0.0387	0.0377	2.65

4.2 Comparison Results for Different Tail Profiles

The model with nose n=3 and Huang tail is considered as the least drag profile combination for the bare hull. It is further required to investigate these models by changing the tail profiles of the hull. The optimum tail profile is obtained by changing the value of semi-tail angle (θ) in the Myring tail equation. Three profiles are considered. The models are then tested with the inclusion of tail profiles to identify the hydrodynamically low drag profile for the bare hull. The CFD simulation has been carried out with the modified hull with different tail profiles. The comparison of the results is shown in Figure 13 and the results are tabulated in Table 5.

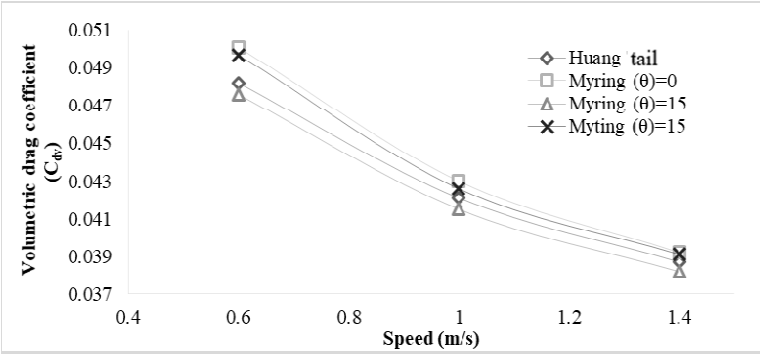

Figure 13: Comparison of Drag Coefficient for Different Tail Profiles

Table 5: Drag Coefficient Values for Different Tail Profiles

Speed (m/s)	Coefficients of Volumetric Drag (C_{dv})			
		For Different Semi-Tail Angle (θ)		
	Huang tail	(θ)=0^0	(θ)=15^0	(θ)=25^0
0.6	0.0482	0.0501	0.0476	0.0497
1	0.0421	0.043	0.0415	0.0426
1.4	0.0387	0.0392	0.0382	0.0391

It can be seen that the tail profile with 15^0 semi-tail angles is the optimum tail with Myring, nose n=3. The results from CFD analysis shows that, the combination of Myring nose (n=3) and Myring tail semi-tail angles (15^0) is having the minimum drag. The comparison of the final AUV model with the modified tail, i. e., 15^0 semi-tail angles are tabulated and presented in Table 6. The percentage deviation indicates that tail profile with (θ) = 15^0 is having lesser drag coefficient values than Huang tail.

Table 6: Comparison of Least Drag tail with Huang Tail

Speed (m/s)	Volumetric Drag Coefficients (C_{dv})		
	Base Model (n=2) and Huang Tail	(θ) = 15^0	Deviation %
0.6	0.0482	0.0476	1.3020
1.0	0.0421	0.0415	1.3374
1.4	0.0387	0.0382	1.3419

5. CONCLUSIONS

In the present investigation, a numerical analysis using the CFD technique has been carried out to obtain the low drag profile for the selected AUV models. This is an initial research work for developing a biomimetic AUV model with higher capabilities of hovering and surveillance for military purpose. The numerical results are first compared and validated with the published research to obtain standard settings in the CFD tool. Various nose and tail profiles have been generated with the Myring equation and further the CFD analysis has been carried out. The Myring nose with n = 3 with semi tail angle of θ, 15^0 is found to be the lowest drag profile among the selected hull forms. In the future, the hull would be modified with biomimetic propulsion with the control surface and experiments to be carried out to validate the developed model.

REFERENCES

1. *Griffiths, G, Technology and Applications of Autonomous Underwater Vehicles, of ocean Science and technology, CRC Press, Pp. 37-38, (2002).*
2. *Mc. Phail S., Ocean Margin Systems, Springer, Verlag Berlin Heidelberg, Germany, pp 79-97 (2000)*
3. *Sighard F. Hoerner, Fluid- Dynamic theoretical, experimental and statistical information New York, USA, (1965).*
4. *Huang, T. T., Santelli, N., Belt, G. Stern boundary-layer flow on axisymmetric bodies. In: Proceedings of the Twelfth ONR Symposium on Naval Hydro-dynamics Washington D. C., pp. 127–157, (1978).*
5. *Jagadeesh P,. Murali K Application of low-Re turbulence models for flow simulations past underwater vehicle hull forms. The Journal of Naval Architecture & Marine Engineering1 (2), 41–54, (2005).*
6. *Jagadeesh P & Murali K (2009). Experimental investigation of hydrodynamic force coefficients over AUV hull form. Ocean Engineering Journal 36:113–118, (2009).*
7. *T Wulff, Thorben Entwicklung eines Wasserprobennahmesystems als wissenschaftliche Nutzlast eines autonomen Tauchfahrzeugs, pp 6, 2009.*
8. *Deshpande, NEELA., Kulkarni, S. S., Pawar, Tejaswinee., & Gunde, Vijay. (2014). Experimental investigation on strength characteristics of concrete using tyre rubber as aggregates in concrete. International Journal of Applied Engineering Research and Development, 4(2), 97-108.*
9. *Phillips, A., M. Furlong. The Use of Computational Fluid Dynamics to Assess the Hull Resistance of Concept Autonomous Underwater Vehicles. IEEE: OCEANS 2007: Europe. Pp. 1-6, (2007).*
10. *Myring D. F, The effect of body shape and Mach number on the drag of bodies of revolution in subcritical axis-symmetric flow. Aeronautical Quarterly, Pg. 186-194, (1976).*
11. *Y N Kormilitsin, O A Khalizev, Theory of Submarine Design, Riviera Maritime Media, pp 272-290, (2001).*
12. *Wu J, Zhang M, Hydrodynamic Characteristics of the Main Parts of a Hybrid Driven `Underwater Glider PETREL. Autonomous Underwater Vehicle Edited by Nuno A. Cruz, InTech, Croatia, pp. 39-64, (2011).*
13. *C. C. Eriksen, T. J. Osse, R. D. Light, T, et al, (2001)"Sea glider: A long range autonomous underwater vehicle for oceanographic research," IEEE Journal of Oceanic Engineering, Vol. 26, 2001, pp. 424–436.*
14. *Ananthakrishnan, P., Zhang, K.-Q. AUV motion in a wave field. In: Proceedings of the IEEE OCEANS'98 Conference, Nice, France, pp. 1059–1063(1998).*
15. *Anil Dash, Panneerselvam, S., Idichandy, V. G., Vendhan, C. P. Multicomponent force measurement on submerged bodies. In: Proceedings of the International Conference in Ocean Engineering COE'96, IIT Madras, India, 17–20 December, pp. 553–557 (1996).*
16. *Choi, S. K., Ching, J. C. Navier–Stokes solution of complete turbulent flow past finite axisymmetric bodies. AIAA Journal 29 (6), 998–1001(1991).*
17. *Suresh, R., & Kumar, M. P. (2013). Investigation of tribological behavior and its relation with processing and microstructures of Al 6061 metal matrix composites. International Journal of Research in Engineering & Technology, 1(2), 91-104.*
18. *Gertler, M. Resistance experiments on a systematic series of streamlined bodies of revolution—for application to the design of high-speed submarines. DTRC (1950).*

19. *Jagadeesh, P., Murali, K. Investigation of alternative turbulence closure models for axisymmetric underwater hull forms. The Journal of Ocean Technology 1 (2), 37–57(2006).*

20. *Phillips, A. B., Furlong, M., and Turnock, S. R. The use of computational fluid dynamics to assess the hull resistance of concept autonomous under-water vehicles. In Proceedings of the OCEANS2007 Europe TS/IEEE conference and Exhibition, Aberdeen, UK, 18–21 June 2007, pp. 1–6(IEEE, New York).*

21. *Stevenson, P., Furlong, M., and Dormer, D. AUV shapes – combining the practical and hydrodynamic considerations. In Proceedings of the OCEANS Europe MTS/IEEE Conference and Exhibition, Aber- deen, UK, 18–21 June 2007, pp. 1–6 (2007).*

22. *Curtis, T. L., Perrault, D., Williams, C., and Bose, N. N-Scout: a general-purpose AUV for systems research. In proceedings of the 2000 International Symposium on Underwater technology, pp. 73–77 (2000)*

23. *Fallows, C. D. Characterization of the propulsion system of autonomous underwater vehicles. PhD Thesis, University of Southampton, Southampton, Hampshire, UK, (2004).*

24. *Pashias, C. Shape optimization of a long range autonomous underwater vehicle using computa- tional fluid dynamics. Ship Science Part III Honors Report SS583, University of Southampton, Southampton, Hampshire, UK, (2001).*

25. *Rathod, Chandar., & Reddy, G. K. (2016). Experimental investigation of angular distortion and transverse shrinkage in CO2 arc welding process. International Journal of Mechanical Engineering, 5(4), 21-28.*

26. *Burcher, R. and Rydill, L. Concepts in submarine design, (Cambridge University Press, Cambridge) (1994).*

27. *Katz, J. and Plotkin, A. Low-speed aerodynamics: from wing theory to panel methods, 1991 (McGraw- Hill, New York)(1991).*

28. *Versteeg, H. K. and Malalasekere, W. An introduction to computational fluid dynamics: the finite volume method, 2nd edition,(Pearson Prentice Hall, Saddle River, New Jersey) (2007)*

29. *G. Stante, M. Nahon and C. D. Williams. Simulation of an underwater glider. In Proceedings of the 15th International Symposium on unmanned untethered submersible Technology conference (UUST'07), Durham, NH, USA, 19 to 20 August. AUSI (2007).*

30. *Inoue, T., H. Suzuki, R. Kitamoto, Y. Watanabe and H. Yoshida.. Hull Form Design of Underwater Vehicle Applying CFD (Computational Fluid Dynamics). OCEANS 2010 IEEE – Sydney. Pp 1-5 (2010).*

31. *Sagala F. and R. Bambang. Development of Sea Glider Autonomous Underwater Vehicle Platform for Marine Exploration and Monitering. Indian Journal of Geo Marine Sciences: Vol. 40, N. 2. Pp. 287-295 (2011).*

32. *Stevenson P., M. Furlong, and D. Dormer. AUV shapes - Combining the Practical and Hydrodynamic Considerations. OCEANS 2007 – Europe. Pp. 1-6 (2007).*